NOTES AND CORRESPONDENCE

Persistent Jet Stream Intensifications: A Comparison between Theory and Data

K. HAINES,* P. MALANOTTE-RIZZOLI, AND M. MORGAN

Center for Meteorology and Physical Oceanography, Massachusetts Institute of Technology, Cambridge, Massachusetts

8 November 1991 and 3 April 1992

ABSTRACT

A diagnostic study of persistent intense jet stream events in the Pacific has been carried out with a 15 winter NMC dataset to assess the relevance of the weakly nonlinear model recently proposed by Haines and Malanotte-Rizzoli. Composited data from 14 episodes of persistent intensification anomalies in the central and eastern Pacific have been analyzed with scatter diagrams of potential vorticity q plotted against geopotential Φ on the 300-mb surface. The slope of the functional relationship gives a measure of the wavelength independent component of the refractive index ($n^2 = -\Lambda_0 = -dq_0/d\psi_0$). The theoretical model suggests that if $dq_0/d\psi_0$ is more negative on the northern and southern flanks, a local intense region within the jet stream may be abnormally persistent. The composited dataset shows that this condition is satisfied during the postonset period as defined by Dole. In contrast, the climatology and the mean flow before onset does not show much variation in Λ_0 across the jet. Results are encouraging, but higher-resolution data is needed to draw firm conclusions.

1. Introduction

A weakly nonlinear theory allowing for local wave solutions to the quasigeostrophic, baroclinic potential vorticity equation was proposed as a model of blocking in a series of studies (Malguzzi and Malanotte-Rizzoli 1984, 1985; Malanotte-Rizzoli and Malguzzi 1987; Malanotte-Rizzoli and Hancock 1987). The basic dynamics of this theory is that of the Korteweg de-Vries (KdV) solitary wave equation. Malguzzi and Malanotte-Rizzoli (1984, hereafter MR84) showed that an isolated split-jet solution could be obtained for realistic atmospheric parameters and suggested that such a solitary wave model may capture the essential dynamics in many cases of atmospheric blocking.

Work by Dole and Gordon (1983) and Dole (1986, 1989) has shown, however, that other distinct localized modes of low-frequency variability also exist in the form of an intensified westerly jet stream occurring in the same regions as the blocking anomalies. The flow configurations leading to jet intensification have persistent anomalies from the time-mean state in the form of a low-over-high dipole in the geopotential height field (Dole's negative height anomalies).

Recently, Haines and Malanotte-Rizzoli (1991, hereafter HMR) extended the theory proposed in MR84 for the split-jet anomalies and showed that persistent intense jet solitary waves could also be found. In the weakly nonlinear model the intensified jet and the split jet appear as two persistent anomaly states consistent with a different cross-stream structure of the "potential" function or the refractive index; $\Lambda = dq/d\psi$, associated with the zonal jet stream. HMR discuss the relevance of the weakly nonlinear theory for both types of anomalies. In the case of the better-known blocking events, the anomalies become highly nonlinear at upper levels as the potential vorticity contours close off; for example, Shutts (1986) and, in this case, the strongly nonlinear modon models of McWilliams (1980), Verkley (1984, 1987), Haines and Marshall (1987), Butchart et al. (1989), and Haines (1989) may be more appropriate. Haines and Marshall argue that the closing of potential vorticity contours marks the formation of a truly local structure that has achieved a degree of independence from the jet stream in which it is embedded such that the refractive index structure of the jet is no longer crucial for persistence. The weakly nonlinear model, however, may still be relevant at early stages of block formation or at lower atmospheric levels, where the potential vorticity contours do not become closed.

The intense jet persistent anomalies do not have a strongly nonlinear analytic analogue that differs fundamentally from the weakly nonlinear model. For these anomalies the potential vorticity contours do not generally become closed at any stage; thus, the weakly nonlinear mechanisms may be important at all atmospheric levels and throughout the event life cycles. Diagnostic tools suggested by the theory of HMR can be used to clarify the relevance of these ideas to the

* *Present affiliation:* Department of Meteorology, Edinburgh University, Edinburgh, United Kingdom.

Corresponding author address: Dr. Keith Haines, Edinburgh University, Department of Meteorology, Edinburgh, EH9 3JZ United Kingdom.

intense jet events in the atmosphere. The basic diagnostic that differentiates between positive and negative height anomaly cases is the Λ_0 function, and this can be obtained by plotting diagrams of potential vorticity q against streamfunction ψ at a given height. In this paper we use this diagnostic to study a composite of intense jet events in the Pacific (the negative height anomaly cases of Dole). The paper is organized as follows. In section 2 we summarize the aspects of the weakly nonlinear theory relevant to the present analysis. In section 3 we show the series of composite Pacific intense jet fields and present the scatter diagram diagnostics. In section 4 we discuss conclusions and directions for future work.

2. The theory

We summarize the theory of weakly nonlinear isolated anomalies following MR84 and HMR. Consider the barotropic potential vorticity equation for stationary, inviscid flow:

$$J(\psi, q) = 0, \tag{1}$$

where ψ is the flow streamfunction, $q = \nabla^2\psi + \beta y$ is the potential vorticity,

$$J(a, b) = \frac{\partial a}{\partial x}\frac{\partial b}{\partial y} - \frac{\partial b}{\partial x}\frac{\partial a}{\partial y}$$

is the Jacobian, and β is the planetary vorticity gradient. Expand the solution as a small-amplitude perturbation about a zonal flow, ψ_0, using the small-amplitude parameter $\epsilon \ll 1$:

$$\psi = \psi_0(y) + \epsilon A(x)\phi(y) + \cdots,$$

where we have assumed the solution at order ϵ is in separable form $\psi_1 = A(x)\phi(y)$. Expanding the potential vorticity similarly and substituting into Eq. (1) gives an eigenvalue problem in the meridional direction:

$$\phi_{yy} + (\lambda - \Lambda_0(y))\phi = 0. \tag{2}$$

The boundary conditions will be $\phi(\pm w) = 0$, with $y = \pm w$ defining the walls of the β-plane channel. The function

$$\Lambda_0 = \frac{dq_0}{d\psi_0} = -\frac{1}{U_0}\frac{dq_0}{dy}$$

has the dimensions of an inverse length scale squared, and Eq. (2) couples the wavenumber of the stationary perturbation with that of the zonal flow. If Λ_0 is constant, then $(-\Lambda_0)^{1/2}$ gives the total wavenumber of a stationary Rossby wave solution. A variable Λ_0 plays the role of a weighting or potential in Eq. (2), and if Λ_0 has a minimum value at some latitude, then the meridional structure eigenfunction ϕ may be localized in this region. Alternatively, as suggested in HMR, the meridional trapping may be provided by critical lines that could act more like the walls at $y = \pm w$ in the simple β channel above. In the zonal direction MR84 show that if λ in Eq. (2) is $O(\epsilon)$, then at the lowest order in ϵ we have

$$A_{xx} - \lambda A + \frac{\delta}{2}A^2 = 0, \tag{3}$$

where the constant δ is given by

$$\delta = -\int_{-w}^{w} \frac{d\Lambda_0}{d\psi_0}\phi^3 dy \Big/ \int_{-w}^{w} \phi^2 dy$$

and the boundary conditions are $A(\pm\infty) = 0$. Equation (3), which assumes a long zonal scale $x = O(\epsilon^{-1/2})$, is the time-independent Korteweg de-Vries equation, and it has soliton solutions, provided $\lambda > 0$, of the form

$$A = \frac{3\lambda}{\delta}\,\mathrm{sech}^2\left(\frac{\lambda^{1/2}}{2}x\right).$$

The anomaly streamfunction at $O(\epsilon)$ is given by $\psi_1 = A(x)\phi(y)$. The sign of A is determined by the sign of δ, since the eigenvalue λ must be positive, and thus, the sign of ψ_1 is given by the sign of

$$\frac{\phi}{\delta} = -\frac{1}{\phi}\int_{-w}^{w} \frac{d\Lambda_0}{d\psi_0}\phi^3 dy.$$

Haines and Malanotte-Rizzoli (1991) show that this requires that Λ_0 be more negative on the flanks of the jet stream than in the center if the jet is to support persistent intensified regions. If Λ_0 is less negative on the jet flanks, then a split-jet stream anomaly can persist. Note that the sign of Λ_0 itself is virtually always negative under atmospheric conditions. HMR constructed intense jet solitons in the barotropic β-channel framework, and an example of such a flow is shown here in Fig. 1a. The scatter-diagram diagnostic was used by HMR to illustrate the important Λ_0 structure associated with the jet, and the q/ψ scatter diagram for the Fig. 1a flow is shown in Fig. 1b. The more negative slope at large negative and positive q values on the jet flanks is very clear. It is emphasized that the curvature in Fig. 1b is a property of the jet and is not the result of the presence of the intense anomaly, although the anomaly can resist dispersion because of this jet characteristic. This figure is reproduced for comparison with the atmospheric data analysis described in the next section.

3. Diagnostic results

a. Dataset

Our data are derived from twice-daily National Meteorological Center Northern Hemisphere final analyses of geopotential heights Φ and temperatures T at all standard levels from 1000 hPa to 100 hPa on a hemispheric grid with resolution of 4° latitude by 5° longitude. The results presented here analyze data from

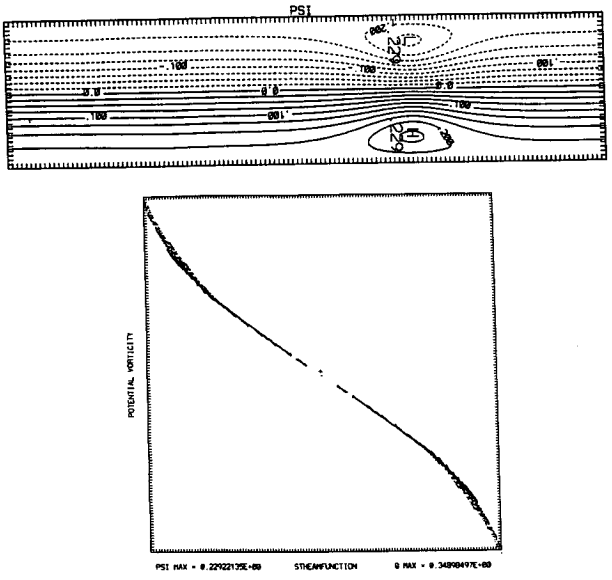

FIG. 1. (a) Streamlines ψ for a quasi-steady intense jet solution in a barotropic β-plane channel. (b) Scatter diagram of potential vorticity q against ψ for the flow shown in (a) [from Haines and Malanotte-Rizzoli (1991)].

the 300-hPa (mb) level, where the midlatitude jet stream is most intense. Isobaric quasigeostrophic potential vorticity q analyses were performed for the Northern Hemisphere region from the pole to 20°N. The q is calculated from the height and temperature data. Centered differencing of the geopotential heights is used to calculate the geostrophic winds $\mathbf{u}_g$:

$$\mathbf{u}_g = \mathbf{k} \times \frac{g}{f} \nabla \Phi, \tag{4}$$

where g is the acceleration due to gravity, f is the latitudinally dependent Coriolis parameter, and $\mathbf{k}$ is a unit vertical vector. Centered differencing is also used to calculate the relative vorticity on isobaric surfaces. Finally, a quadratic interpolant is used to determine the temperature profile for the baroclinic contribution to q. The full expression is

$$q = f + \mathbf{k} \cdot \nabla \times \mathbf{u}_g + f \frac{\partial}{\partial p}\left(\frac{T'}{S}\right), \tag{5}$$

where T' is the thermal perturbation from the average on isobaric surfaces. The static stability term S also represents a horizontal average of the climatological static stability poleward of 22°N at the appropriate pressure level.

b. The climatological state

To identify positive and negative persistent anomalies, a climatology must first be defined that can then be subtracted from the instantaneous atmospheric state. This climatology is a winter seasonal mean, computed by averaging at each grid point all the data from 15 winters in the period 1966–80. The winter season is defined as the 120 days following 15 November each year.

Figure 2a shows the climatological mean 300-mb geopotential height in meters (solid lines) and the corresponding potential vorticity (dashed lines) in units of 10^{-5} s^{-1}. The fields show considerable zonal asymmetry due to orography and land–sea thermal contrasts. The key region for Pacific negative anomalies is through the western and central North Pacific, and this region covering 38°–54°N, 145°E–175°W is outlined bold on the climatological map. The southerly extent of this region is limited by uncertainty in how to best define q across a wide latitudinal range and near strong jets where spuriously negative q values can easily occur. The northerly limit spans the intense jet region so that points north of 54° are in a stagnant region, where weakly nonlinear theory would be inappropriate. During persistent anomaly periods the jet intensifies and shifts its position from its maximum at around 145°E off the coast of Japan out into the central Pacific and across the date line before beginning to weaken in the east Pacific (Fig. 3a).

Data from the key region in Fig. 2a was plotted on a scatter diagram of q against a scaled geopotential coordinate in Fig. 2b. The scaled geopotential, x, is defined below:

$$x = \frac{\Phi - 8750 \text{ m}}{450}, \tag{6}$$

which ensures that the range of x within our region varies approximately between -1 and $+1$. The reason for the scaling is made clear in the following. An almost linear functional relationship is evident from the points on the scatter diagram. We wish to make some judgment of the slope variations in later diagrams, and therefore, the points are fitted to a cubic polynomial function using a least-squares distance criterion, and the line through the points in Fig. 2b is the best-fitting cubic whose equation is given at the top of the graph (y: potential vorticity; x: scaled geopotential). The scaling ensures that the coefficients in the polynomial are all scaled to a value of 1. A measure of the tendency toward increasingly negative gradients at high and low potential vorticity values (i.e., on the northern and southern jet flanks) is given by the negativity of the coefficient of x^3 in the functional relationship. This cubic component will be seen to increase considerably in cases of intense jet persistence. A very slight curvature in the climatology diagram is visible in the polynomial and is consistent with previous scatter diagram results; for example, Marshall and So (1990, Fig. 3). The curvature is of the same sign as Fig. 1b, with increasingly negative gradients at the line extremities (on the N and S jet flanks) suggesting that the climatological

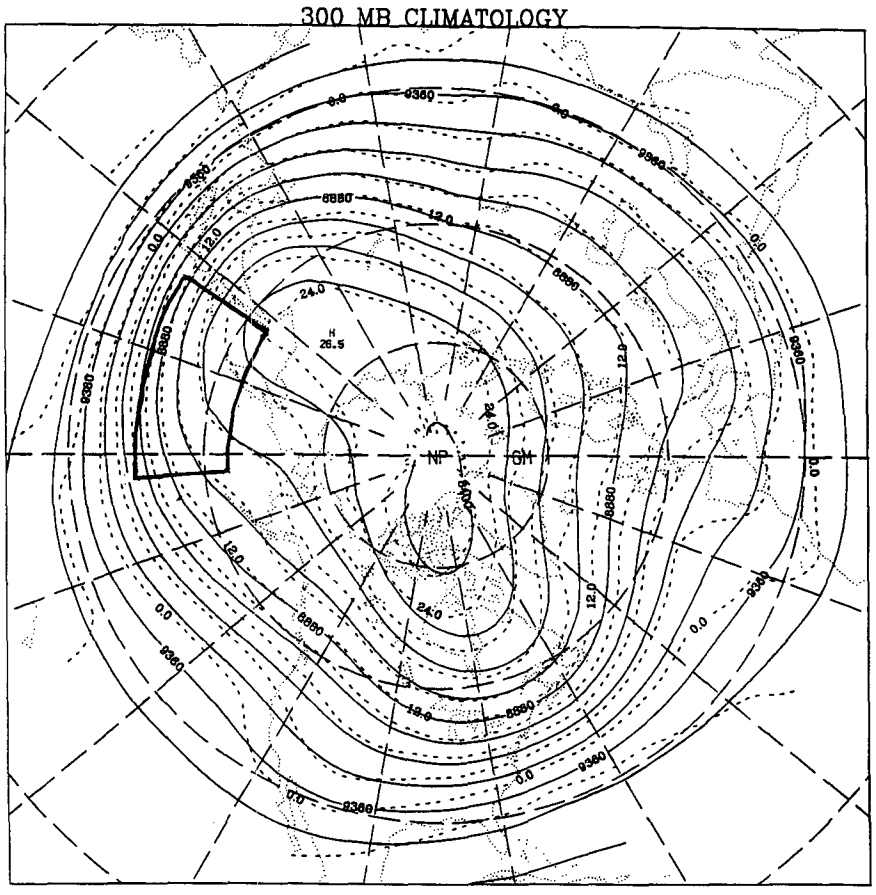

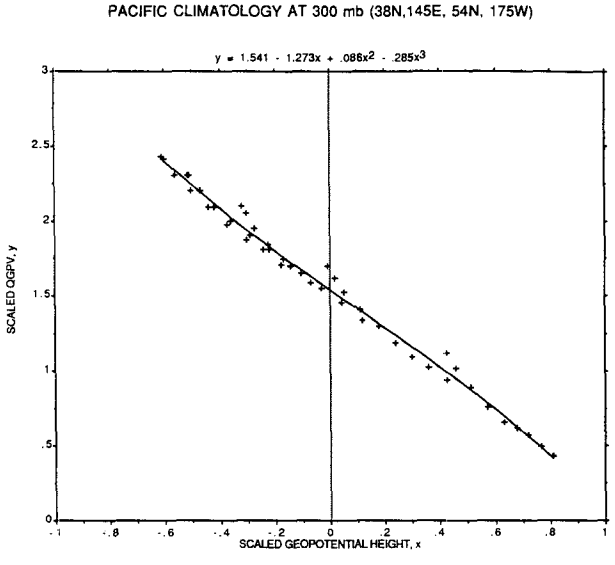

FIG. 2. (a) The geopotential height (solid lines) and quasigeostrophic potential vorticity (dashed lines) of the 300-mb Northern Hemisphere wintertime climatology (see text for details). The key region for the Pacific intense jet anomalies is outlined bold. Contour intervals, $\Phi = 120$ m, $q = 3 \times 10^{-5}$ s^{-1}. (b) Scatter diagram from the key region in (a) with scaled Φ (see text). Units of q are 10^{-4} s^{-1}; units of Φ are 450 m.

winter jet may normally show some slight preconditioning for the support of intense jet-type anomalies. Alternatively, it may reflect the inclusion of a number of Pacific negative cases in the climatological jet average.

c. *Persistent anomalies*

We have used the persistent anomaly dataset obtained by Dole and Gordon (1983) as the basis for this study and have focused on the Pacific negative anomalies for comparison with the weakly nonlinear intense

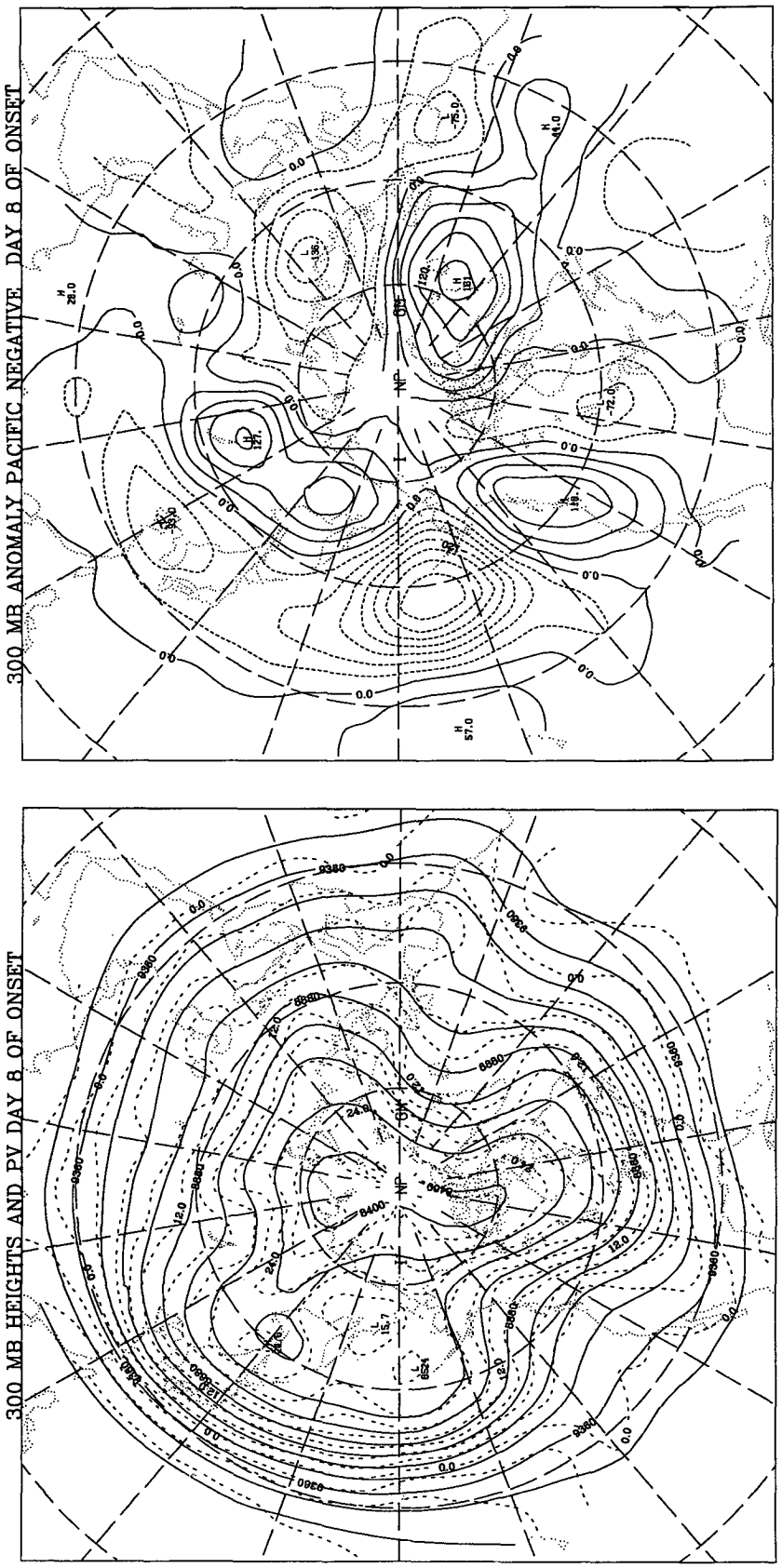

FIG. 3. (a) Composite fields at day +8 after onset of Pacific negative anomalies. Solid lines are geopotential height; dashed lines are potential vorticity. Units as in Fig. 2a. (b) Composite anomaly geopotential field at day +8 after onset. A strong negative anomaly and a weak positive anomaly to the south span the date line, intensifying the jet in between. Contours of Φ are 30 m apart.

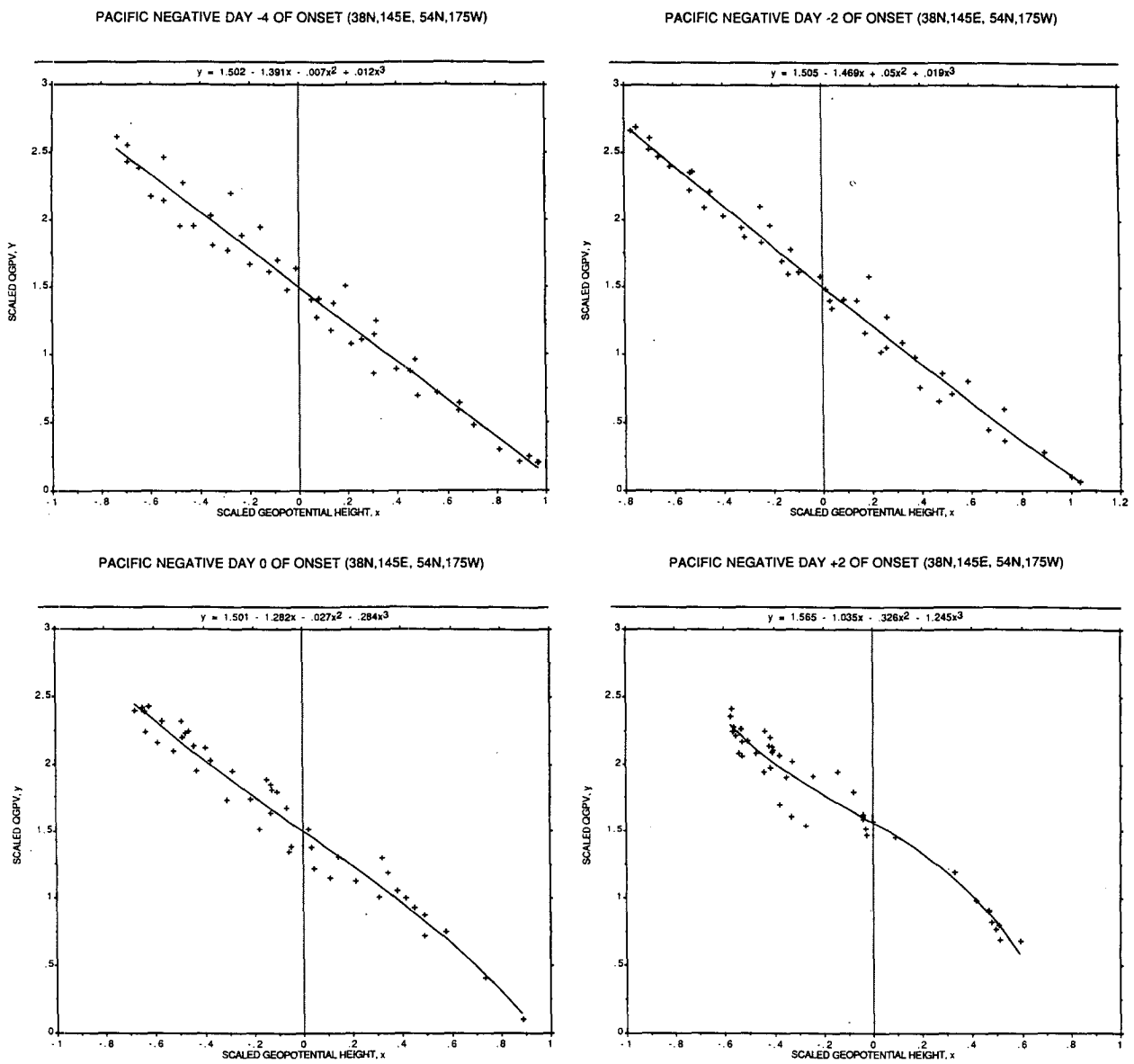

FIG. 4. Scatter diagrams of q against scaled geopotential within the key region for the composite fields on days -4 to $+10$ of onset time, (a)–(h), respectively. Units are as in Fig. 2b.

jet structures described in HMR. The persistent anomalies satisfy amplitude and duration criteria such that the anomaly must have an amplitude, $\Phi' \geq 100$ m on the 500-mb surface, and a persistence time, $t \geq 10$ days. The negative height anomalies studied here are associated with intense jet events over the North Pacific centered on Dole's "key point" (45°N, 170°W), and their structure and life cycles are described and catalogued in Dole (1989).

To construct scatter diagrams for these events that are capable of revealing a functional relationship between potential vorticity and geopotential, a composite of fields is taken from a number of events so as to capture reproducible features that characterize intense jet anomalies. Dole (1986, 1989) made extensive use of composited data for analyzing the development of persistent anomalies, and Malanotte-Rizzoli and Hancock (1987) used composited data to study potential function variations during positive anomaly split-jet stream events. The composite analyses are obtained from an ensemble of 14 individual cases that occurred during the 15 winter period, with the averaging performed with respect to the day of "onset" of the anomaly when the anomaly geopotential amplitude first crosses the 100-m threshold on the 500-mb surface. This day is labeled "day zero," and time is measured

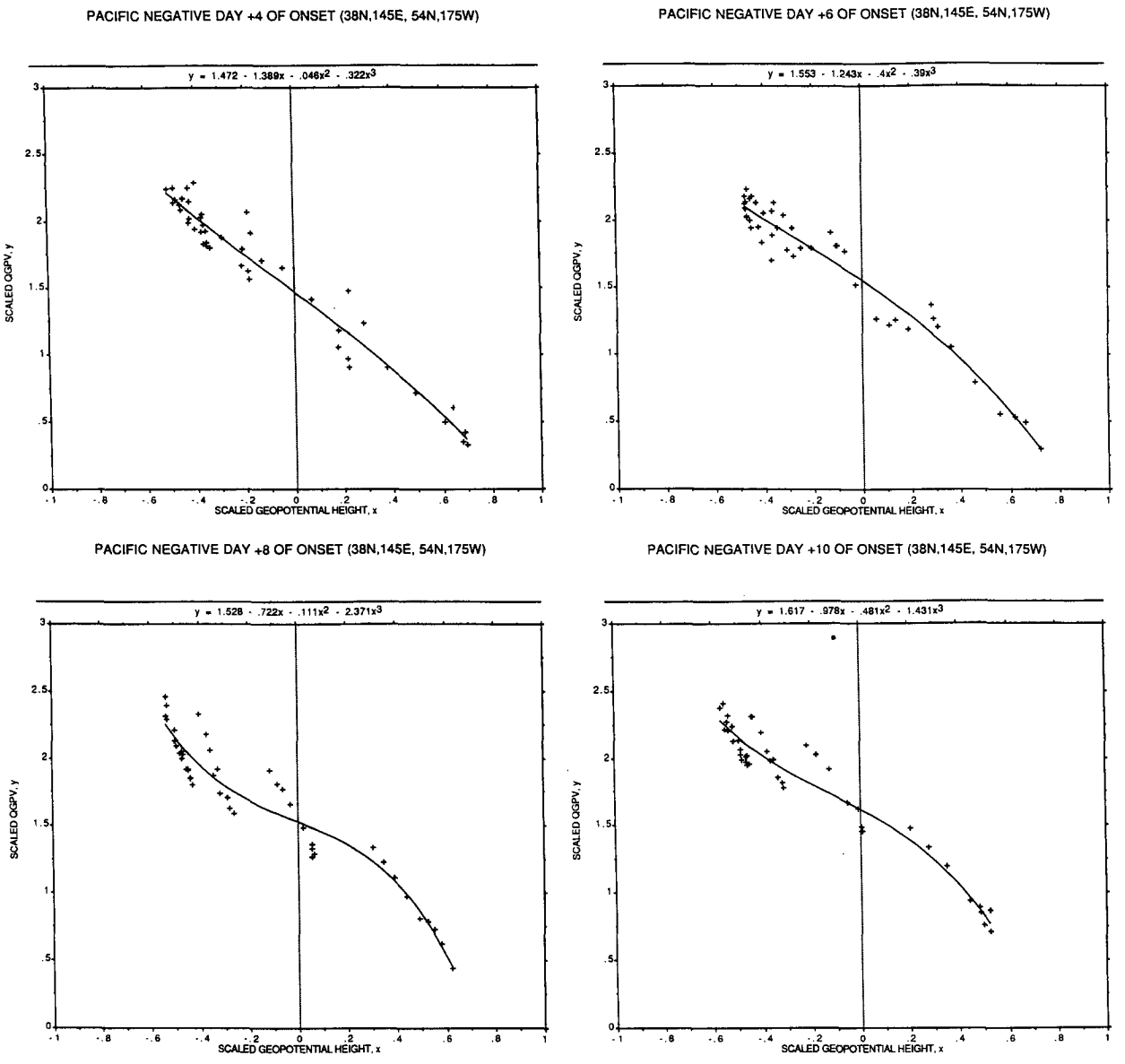

FIG. 4. (*Continued*)

relative to this day. Thus, day −2 represents the time two days prior to the onset; day +2, two days after the onset. Composite fields are then constructed by averaging the fields from all 14 anomaly events on day 0, or on day +2, for example.

Figure 3a shows the 300-mb height field composite on day +8 for the intense Pacific jet cases, and Fig. 3b shows the associated height anomaly from the climatology. These figures give an impression of the structure of the mature phase of the persistent intense-jet anomalies in the Pacific with an extended cyclonic anomaly stretching through the key region that pinches and intensifies the jet through the central Pacific and across the date line. A much weaker high to the south can also be seen in the geopotential anomaly map, and although this would appear stronger in the streamfunction, the symmetric dipoles; for example, Fig. 1a, do not appear to be very realistic here. The theory, however, permits more asymmetric structures for the second eigenfunction of (2) if $\Lambda_0(y)$ were also more asymmetric. We therefore proceed to look for variations in refractive index across the jet that provides the central prediction from the weakly nonlinear theory. We show scatter diagrams at 300 mb for the quadrant defined by 38°N to 54°N; 145°E to 175°W where the Pacific negative anomalies are most intense. The diagrams are constructed for different days of anomaly evolution. Figures 4a–h show scatter diagrams for days

−4 (a); −2 (b); 0, onset (c); +2 (d); +4 (e); +6(f); +8(g); and +10 (h).

Before onset, the best-fitting functional relationships between potential vorticity and geopotential height are quite closely linear, with small coefficients for the higher-order polynomial terms, x^2 and x^3. If anything, there appears to be less curvature in Figs. 4a and 4b than in the climatology, Fig. 2b, suggesting perhaps that the climatological curvature is due to averaging through intense jet events. At onset, day 0, a slight tendency for the slope to become more negative at the two extremities of the line is apparent. The cubic term in the best-fit functional relation, shown at the top of each plot, switches from positive to negative at this time and increases in size by a factor of about 15 over the value on day −2. After onset, on day +2, the slope at the line extremities is very obviously more negative than at the center and is also considerably more negative than the slope for the climatology. The cubic coefficient in the polynomial has increased again and is now almost two orders of magnitude greater than at pre-onset times. This increased curvature also persists through all the scatter diagrams to day +10, although on days +4 and +6 it is less marked or is concentrated at the low potential vorticity end of the scale indicating the southern jet flank. On the northern flank (high potential vorticity values) there is more spread in the data and the highest q values are less than those on day +2, indicating perhaps that the northern edge of the jet is not being sampled well. Extending the sampling region 4° farther north, however, introduces an area of reversed q gradients, as seen in Fig. 3a, and the interpretation of the results in terms of weakly nonlinear theory becomes more doubtful.

To further demonstrate the differences in the jet structure before and after the onset times we take another average of the composite fields. Figure 5a shows the average geopotential and potential vorticity fields for all the days from −5 of onset to day 0 of onset for the Pacific negative events. Figure 5b shows the average fields for the days +1 to +10 of onset. Figures 6a,b show the corresponding scatter diagrams of potential vorticity against the scaled geopotential for these two periods, pre- and postonset in the key regions. The scatter diagrams clearly show the change that occurs around onset time with the increase in curvature at the northern and southern jet extremities, which are very reminiscent of Fig. 1b from the weakly nonlinear model.

4. Discussion

We have presented some tentative evidence for changes in the potential or refractive index function of the 300-mb jet stream at times when persistent intense jet conditions exist over the central Pacific area. These changes are revealed by the changes of slope in the best-fit functional curve relating the potential vorticity and geopotential heights. The observations are, by and large, consistent with the weakly nonlinear model for intense jet persistence recently proposed by Haines and Malanotte-Rizzoli (1991), with high values of refractive index (low potential function) on the jet flanks that produce a zonally confined region of high refractive index when the jet is pinched together. Haines and Malanotte-Rizzoli have shown that nonlinearity will counteract dispersion under these conditions and hence encourage the persistence of the anomaly. These results are not consistent with the other prototype model for persistent anomalies, the modon (with or without rider), which necessarily has closed q contours and a multivalued $q(\psi)$ functional relationship, neither of which are evident from our observations.

The difficulties of making and interpreting refractive index measurements is well known (see, for example, Randel 1988), and given the low spatial resolution of the data, we have attempted only a qualitative comparison with theory. The principal limitations are the resolution in the meridional direction (4°) and, particularly, the necessity for calculating the relative vorticity from this dataset, which requires the velocity fields to be differentiated. The use of scatter diagrams avoids the need to calculate higher derivatives explicitly by providing a graphical interpretation of refractive index variations. The limited dataset also provides only a small number of points covering the central Pacific region, and this data may be of poor quality due to the lack of genuine observations that require data extrapolation based on numerical models. Another source of uncertainty is in the use of a large-scale average of the static stability for calculating the stretching component of the potential vorticity within the quasigeostrophic framework.

Because of these problems, we hesitate to draw strong conclusions from our results about the validity of the weakly nonlinear model of persistent intense jets. The findings are not inconsistent with the theory, and we believe that enough data is present to establish the credibility of the observed changes in refractive index structure. The data has been composited so that the features retained are consistently present in 14 event cases over a 15-year period. The fitting of a cubic polynomial to the data using a least-square distance criteria makes the interpretation of the plots more objective, if not truly quantitative, since the number of points used for any fit is only 45. The additional averaging of fields for all pre- and postonset days, however, provides a dataset composed of an 84 field average at preonset and 126 field average at postonset times for Figs. 5 and 6.

Although the lack of apparent refractive index variations prior to onset of the intense anomalies is discouraging, as far as the predictive content of the theory goes, it is possible that studies of individual cases may reveal such a prior change. This is because the definition of "onset" used by Dole fixes the central location of the anomalies around the "key point" (45°N, 170°W) on day 0. Therefore, during the individual cases, the jet position and meridional refractive index

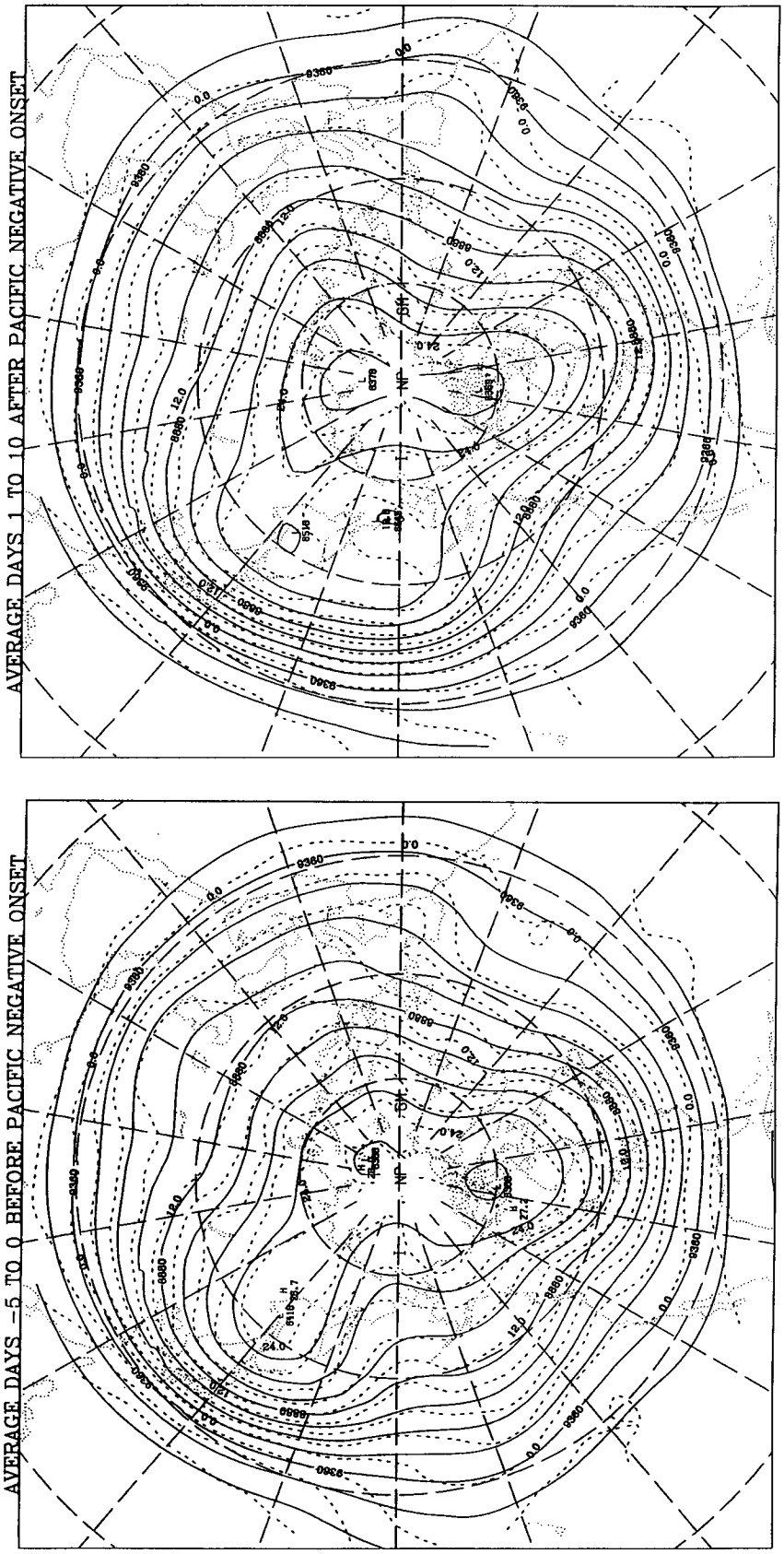

FIG. 5. Mean geopotential (solid lines) and q (dashed lines) for all the days from −5 to onset day 0, (a), and for all the days from +1 to +10 of onset time inclusive, (b). Units as in Fig. 2a.

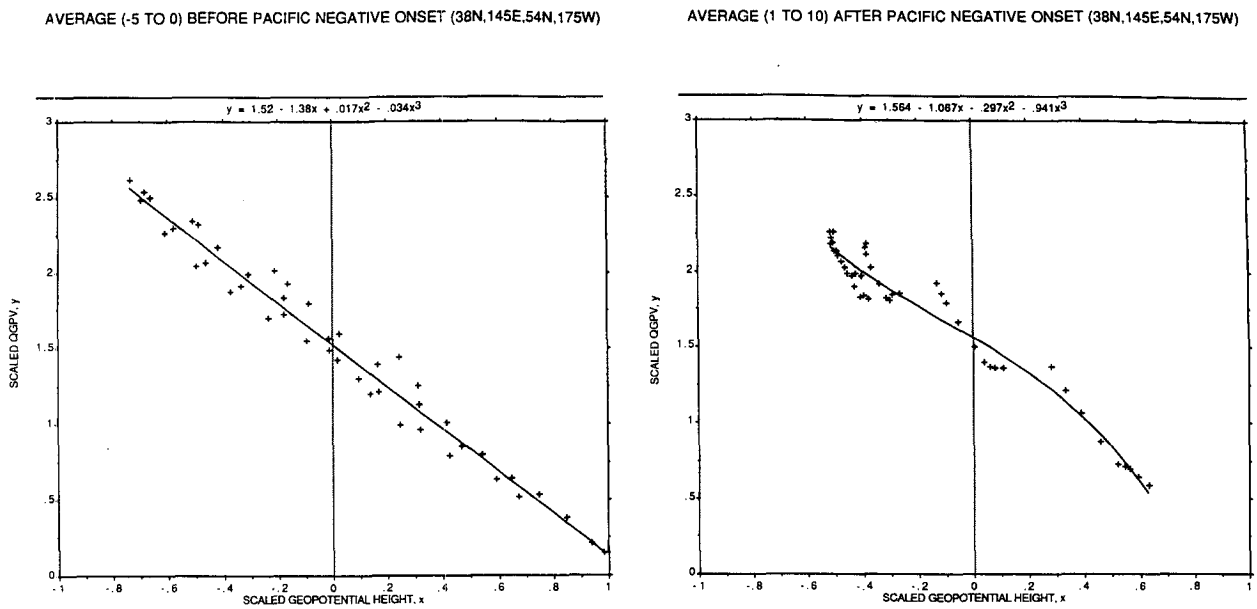

FIG. 6. Scatter diagrams of q against scaled Φ for the mean of composite fields -5 to 0 of onset, (a), corresponding to the fields shown in Fig. 5a, and for days $+1$ to $+10$ of onset inclusive, (b) corresponding to the fields shown in Fig. 5b. Units are as in Fig. 2b.

structure are likely to be well correlated spacially. The latitude of the jet streams prior to each onset, however, may show considerable variation. When the data is composited the meridional refractive index structure may be spread out, leading to the smoothing and straightening of the best-fit curves on the scatter diagrams.

In summary, the HMR theory of persistent intense jets is, so far, the only model proposed to explain the existence of these structures. The model makes firm predictions about the refractive index structure of the jet stream, and although the dataset is of very low resolution, the results presented here are consistent with the HMR model predictions during Dole's negative anomaly events. To make a more accurate analysis and comparison with the theory, a higher-resolution dataset is needed with at least a 2° resolution in the meridional direction. Individual case events may also be worth studying with scatter diagrams, since a feature of Pacific negative anomaly cases is the reduced synoptic activity within the jet that may allow an instantaneous measure of refractive index. Also, in individual cases, prior changes in refractive index structure might be detected that could then be used as a likelihood predictor for intense jet events.

Acknowledgments. This work was supported by NSF Grant ATM 8820938.

REFERENCES

Butchart, N., K. Haines, and J. C. Marshall, 1989: A theoretical and diagnostic study of solitary waves and atmospheric blocking. *J. Atmos. Sci.*, **46**, 2063–2078.

Dole, R. M., 1986: Persistent anomalies of the extratropical Northern Hemisphere wintertime circulation: Structure. *Mon. Wea. Rev.*, **114**, 178–207.

——, 1989: Life cycles of persistent anomalies. Part I: Evolution of 500 mb height fields. *Mon. Wea. Rev.*, **117**, 177–211.

——, and N. D. Gordon, 1983: Persistent anomalies of the extratropical Northern Hemisphere wintertime circulation: Geographical distribution and regional persistence characteristics. *Mon. Wea. Rev.*, **111**, 1567–1586.

Haines, K., 1989: Baroclinic modons as prototypes for atmospheric blocking. *J. Atmos. Sci.*, **46**, 3202–3218.

——, and J. C. Marshall, 1987: Eddy-forced coherent structures as a prototype for atmospheric blocking. *Quart. J. Roy. Meteor. Soc.*, **113**, 681–704.

——, and P. Malanotte-Rizzoli, 1991: Isolated anomalies in westerly jetstreams: A unified approach. *J. Atmos. Sci.*, **48**, 510–526.

McWilliams, J. C., 1980: An application of equivalent modons to atmospheric blocking. *Dyn. Atmos. Oceans*, **5**, 43–66.

Malanotte-Rizzoli, P., and P. J. Hancock, 1987: Coherent structures in a baroclinic atmosphere. Part IV: A comparison between theory and data. *J. Atmos. Sci.*, **44**, 2506–2529.

——, and P. Malguzzi, 1987: Coherent structures in a baroclinic atmosphere. Part III: Block formation and eddy forcing. *J. Atmos. Sci.*, **44**, 2493–2505.

Malguzzi, P., and P. Malanotte-Rizzoli, 1984: Nonlinear stationary Rossby waves on nonuniform zonal winds and atmospheric blocking. Part I: The analytical theory. *J. Atmos. Sci.*, **41**, 2620–2628.

——, and P. Malanotte-Rizzoli, 1985: Coherent structures in a baroclinic atmosphere. Part II: A truncated model approach. *J. Atmos. Sci.*, **42**, 2463–2477.

Marshall, J. C., and D. K. W. So, 1990: Thermal equilibration of planetary waves. *J. Atmos. Sci.*, **47**, 963–978.

Randel, W. J., 1988: The seasonal evolution of planetary waves in the Southern Hemisphere stratosphere and troposphere. *Quart. J. Roy. Meteor. Soc.*, **114**, 1385–1409.

Shutts, G. J., 1996: A case study of eddy forcing during an Atlantic blocking episode. *Adv. Geophys.*, **29**, 135–162.

Verkley, W. T. M., 1984: The construction of barotropic modons on a sphere. *J. Atmos. Phys.*, **41**, 2492–2504.

——, 1987: Stationary barotropic modons in westerly background flows. *J. Atmos. Phys.*, **44**, 2383–2398.